ARTICLE OPEN

Check for updates

An extratropical window of opportunity for subseasonal prediction of East Asian summer surface air temperature

Jing Yang[1]✉, Tao Zhu[1] and Frederic Vitart[2]

Previous studies suggest that boreal summer intraseasonal variations along the subtropical westerly jet (SJ), featuring quasi-biweekly periodicity, frequently modulate downstream subseasonal variations over East Asia (EA). Based on subseasonal hindcasts from six dynamical models, this study discovered that the leading two–three-week prediction skills for surface air temperature (SAT) are significantly higher in summer with stronger intraseasonal oscillation along the SJ, which are best demonstrated over the eastern Tibetan Plateau, Southwest Basin, and North China. The reasons are that the enhanced quasi-biweekly wave and its energy dispersion along the SJ cause more regular quasi-biweekly periodic variations of downstream SAT, which potentially increase regional predictability. This study suggests that the strengthened intraseasonal periodic signals along the SJ would enhance the subseasonal predictability in downstream regions, which could provide a window of opportunity for achieving better subseasonal prediction for EA SAT.

npj Climate and Atmospheric Science (2023)6:46 ; https://doi.org/10.1038/s41612-023-00384-5

INTRODUCTION

Subseasonal prediction, which is crucial for many sectors of society and for decision makers in terms of improved planning and preparations for saving lives, protecting property, and increasing economic vitality[1], is a challenging task in operational service[2,3]. One current barrier to improved subseasonal prediction is the sources of predictability on this time scale. Previous studies have attempted to identify the subseasonal prediction sources, including tropical intraseasonal oscillations (e.g., the Madden–Julian Oscillation (MJO) and boreal summer intraseasonal oscillation (BSISO)), anomalous signals from land (soil moisture and soil temperature), snow cover, sea ice, the stratosphere, and the ocean (e.g., the El Niño–Southern Oscillation (ENSO), local sea surface temperature, and mesoscale sea surface temperature variability), which have all been reviewed comprehensively in the National Academies of Sciences report[1] and Merryfield et al.[4].

Skillful subseasonal prediction is particularly important over East Asia (EA), which is one of the most densely populated regions globally, accounting for 22% of the world's population[5]. Subseasonal prediction in boreal summer over EA is challenging owing to complex interactions between tropical monsoon variability and mid–high-latitude circulation systems[6,7]. Previous studies demonstrated that subseasonal prediction sources over EA include preferable phases of the MJO[8] and BSISO[9], the ENSO state[10], snowpack[11,12], land surface conditions[13–15] and stratospheric signals[16]. Conventional perspective considers the extratropical atmospheric perturbation as noise for prediction[17,18]. However, along the subtropical westerly jet (SJ), remarkable periodic atmospheric intraseasonal signals, such as a quasi-biweekly oscillation, have been proven to have significant influence on the weather and climate of EA[19–21] and even to trigger extreme events[22–24]. Meanwhile, a number of recent studies have found that subseasonal prediction biases over EA are affected substantially by extratropical intraseasonal oscillations along the SJ (EISO-SJ)[25–27]. Therefore, it is worth investigating whether the atmospheric EISO-SJ, similar to the MJO/BSISO, is one of the subseasonal prediction sources over EA.

Considering the atmospheric EISO-SJ features remarkable year-to-year variation in boreal summer (Supplementary Fig. 1 presents a simple example examining the year-to-year variation of the intraseasonal SJ index, calculated in accordance with the definition of Yang and Zhang[28]), the objective of this study was to investigate whether there exists remarkable dependence of EA subseasonal prediction on the atmospheric EISO-SJ from the perspective of comparing summers with strong and weak EISO-SJ intensity, primarily based on the subseasonal-to-seasonal (S2S) hindcast dataset. The results presented in this paper are analyzed in an attempt to identify another important window of opportunity for EA subseasonal prediction.

RESULTS

Remarkable year-to-year variation in EISO-SJ intensity

Similar to some previous studies on the year-to-year variation of intraseasonal oscillation[29–31], EISO-SJ intensity is measured by the standard deviation of boreal summer quasi-biweekly 200 hPa meridional wind (V200) averaged over the SJ core region (35°–43°N, 83°–98°E; shown by the black rectangle in Fig. 1b), i.e., the maximum center of both quasi-biweekly V200 variance and fractional variance (nearly 45% of the total variance) (Fig. 1a, b). In this study, V200 was chosen as the typical variable for representing the EISO-SJ because it features more prominent intraseasonal signals than other circulation fields (e.g., 200 hPa geopotential height (GHT200) and zonal wind (U200)) along the SJ (Supplementary Fig. 2a–f). The quasi-biweekly component was extracted to represent intraseasonal V200 because it is the most dominant intraseasonal periodicity according to the power spectra of the circulation fields along the SJ (Supplementary Fig. 2g).

Figure 1c displays the year-to-year variation of EISO-SJ intensity. To examine the contribution of this year-to-year variation, the original SJ intensity is calculated, which is measured by the

[1]Key Laboratory of Environmental Change and Natural Disaster/Faculty of Geographical Science, Beijing Normal University, Beijing 100875, China. [2]European Centre for Medium-Range Weather Forecasts (ECMWF), Reading, UK. ✉email: yangjing@bnu.edu.cn

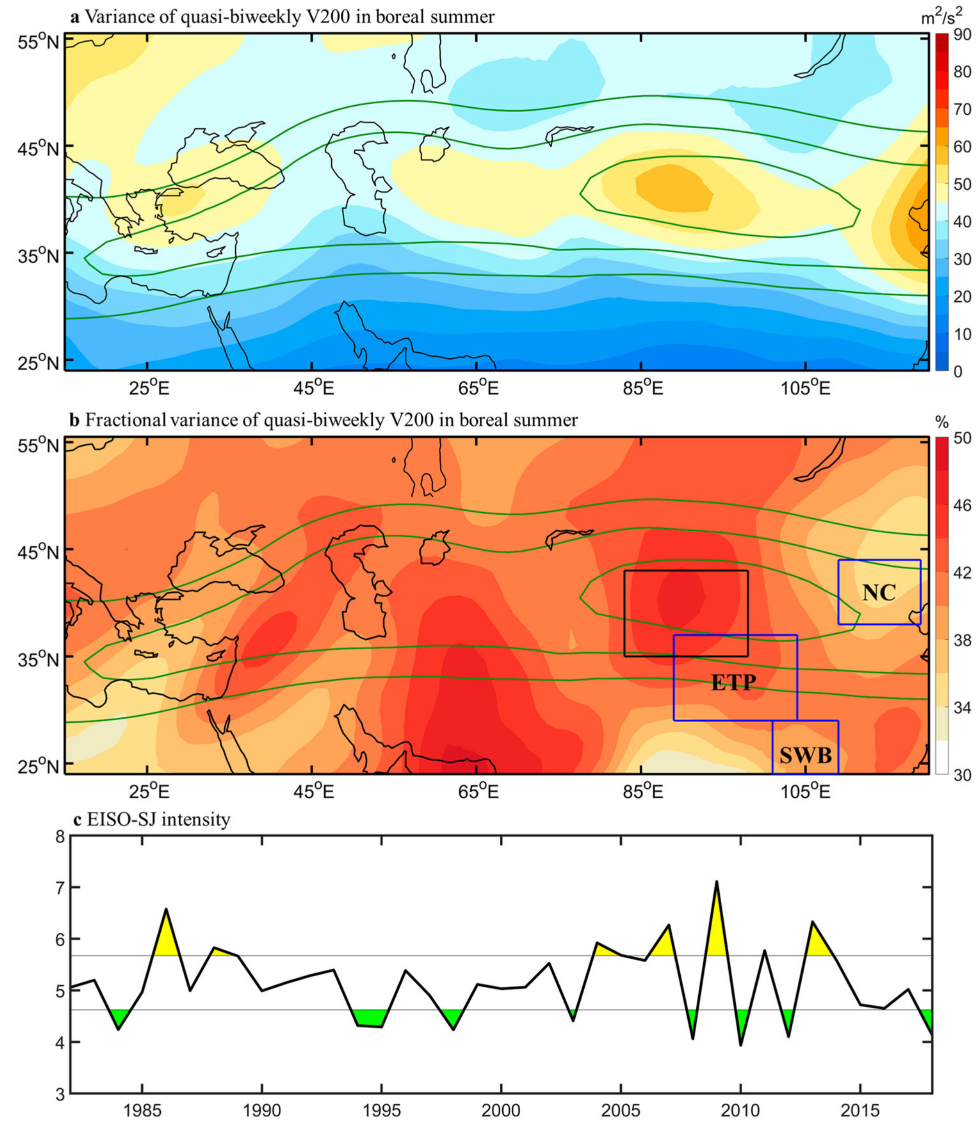

Fig. 1 Intraseasonal activity along the SJ and the year-to-year variation of EISO-SJ intensity. **a** Variance (shading; unit: $m^2\ s^{-2}$) of quasi-biweekly V200 in boreal summer during 1982–2018. Green lines are the summer–mean U200 contours of 18, 23 and 28 $m\ s^{-1}$, which broadly denote the SJ's location. **b** Fractional variance (shading; unit: %) of quasi-biweekly V200 against total V200 variance in boreal summer. Green lines are the summer–mean U200 contours of 18, 23 and 28 $m\ s^{-1}$, which broadly denote the SJ's location. The black rectangle is the SJ core region (35°–43°N, 83°–98°E), which is the maximum center of both quasi-biweekly V200 variance and fractional variance. The blue rectangles are the typical EA regions (eastern Tibetan Plateau (ETP): 29°–37°N, 89°–104°E, Southwest Basin (SWB): 24°–29°N, 101°–109°E, and North China (NC): 38°–44°N, 109°–119°E). **c** Time series (unit: $m\ s^{-1}$) of EISO-SJ intensity measured by the standard deviation of boreal summer quasi-biweekly V200 averaged over the SJ core region. Values greater (less) than 0.7 times the standard deviation are shaded yellow (green).

standard deviation of boreal summer raw V200 averaged over the same SJ core region. It's found that the difference between the maximum and minimum value is 3.18 for the EISO-SJ intensity, which represents 72.5% of the difference for the original SJ intensity (4.39). Moreover, EISO-SJ intensity has a significant relationship with the year-to-year change in the original SJ intensity, for which the correlation coefficient is up to 0.51, far exceeding the 99% significance level. Meanwhile, the year-to-year fractional variance of EISO-SJ intensity (variance: 0.56 $m^2\ s^{-2}$) against the original SJ intensity (variance: 0.87 $m^2\ s^{-2}$) is 64.0%. The above results show that EISO-SJ intensity has large year-to-year variation that is highly consistent with the year-to-year variation of original SJ intensity.

To probe the dependence of EA subseasonal prediction on the atmospheric EISO-SJ, two contrasting groups of summers were evaluated for each specific S2S model: strong EISO-SJ summers (EISO-SJ-S) and weak EISO-SJ summers (EISO-SJ-W). Taking the ECMWF as an example, because the reforecast period is 1996–2015 and the frequency of initialization is twice a week, the five strongest EISO-SJ intensity summers (2004, 2007, 2009, 2011, and 2013) in terms of the observations were chosen for the EISO-SJ-S group, and the five weakest EISO-SJ intensity summers (1998, 2003, 2008, 2010, and 2012) in terms of the observations were taken as the EISO-SJ-W group. The sample size of each group was 175 (5 years × 35 times $year^{-1}$), and the TCC, RMSE and ROC are respectively calculated for ensemble-mean weekly SAT/precipitation anomaly in each group. Analysis for the other models followed similar methods and detailed descriptions can be found in Supplementary Table 1. To ensure distinct differences between the two groups and to maintain adequate sample sizes, the selected EISO-SJ-S and EISO-SJ-W summers exceeded a threshold of at least 0.7 times the standard deviation. To exclude

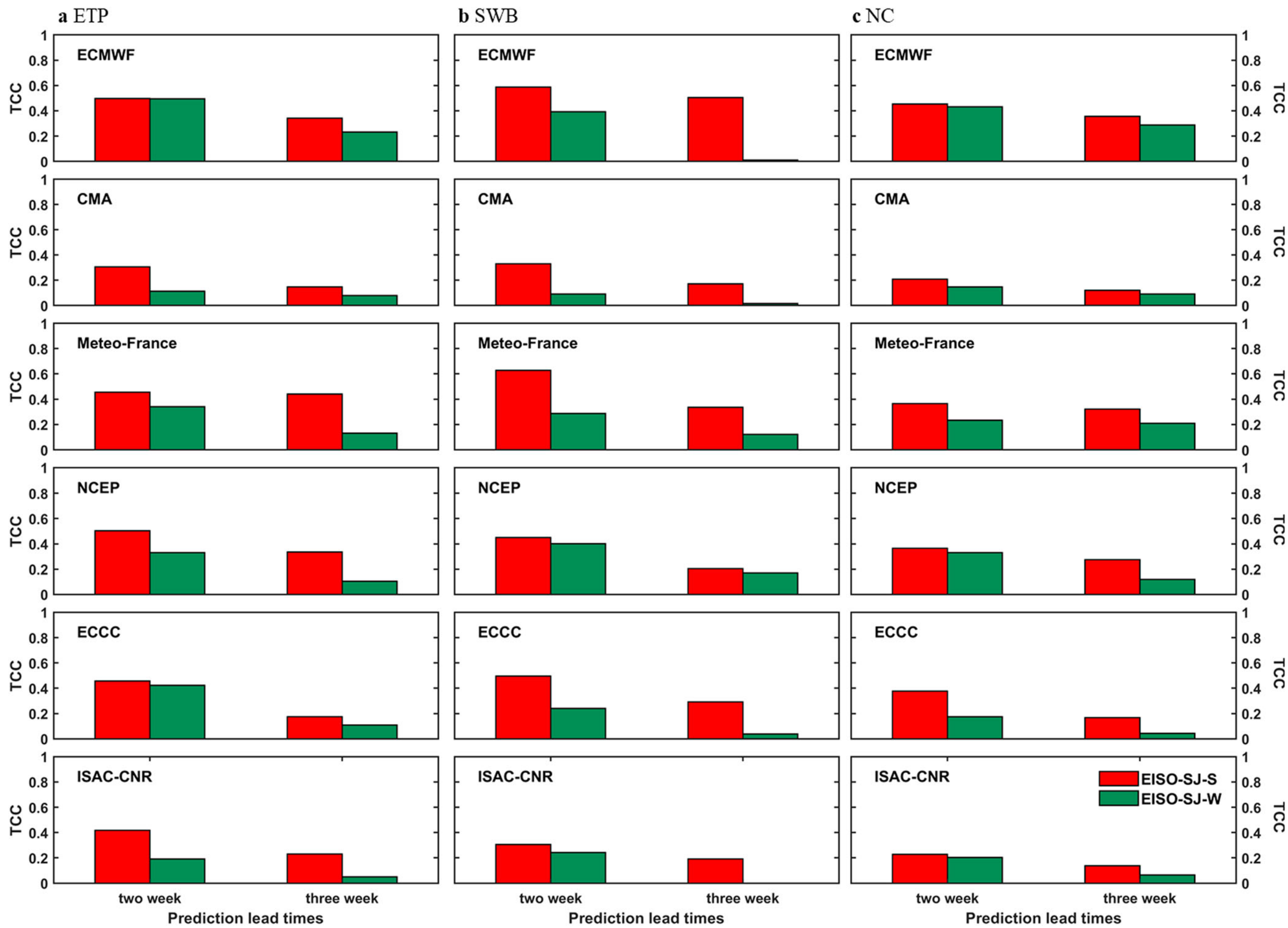

Fig. 2 Subseasonal deterministic prediction over individual typical EA regions: temporal correlation coefficient (TCC). TCC between the observed weekly SAT anomaly and the predicted ensemble-mean weekly SAT anomaly over the (**a**) ETP, (**b**) SWB, and (**c**) NC with two- and three-week lead times. The red (green) bars show the TCC for EISO-SJ-S (EISO-SJ-W) group.

the influence of transient intraseasonal oscillations from the tropical region, we purposely examined the difference in the intensity of the intraseasonal signials (quasi-biweekly and 30–60-day oscillation) between EISO-SJ-S and EISO-SJ-W summers (Supplementary Fig. 3) and found no any significant signals in the tropics.

Dependence of EA subseasonal prediction on the EISO-SJ

Previous observational studies reported that atmospheric EISO-SJ is crucial for subseasonal variation in EA SAT[32–34]. Therefore, in this section, we first focus on exploring the differences in the subseasonal prediction skill for EA SAT between the EISO-SJ-S and EISO-SJ-W summers. Comparison is made for both deterministic (TCC and RMSE) and probabilistic prediction (ROC) to verify the results. Two- and three-week lead predictions are the focuses of this study because the skill beyond four weeks is poor for both groups of summers. Three typical regions are chosen (eastern Tibetan Plateau (ETP): 29°–37°N, 89°–104°E, Southwest Basin (SWB): 24°–29°N, 101°–109°E, and North China (NC): 38°–44°N, 109°–119°E; blue rectangles in Fig. 1b) because the raw SAT anomaly over these regions exhibits significant correlation with the domain-averaged quasi-biweekly V200 over the SJ core (Supplementary Fig. 4).

The TCC and RMSE were calculated to measure the similarity and magnitude of the error between the predicted and observed weekly SAT anomaly[35]. Figure 2a–c shows the TCCs between the observed weekly SAT anomaly and the predicted ensemble-mean anomalies with two- and three-week lead times from the six S2S models over the ETP, SWB, and NC in EISO-SJ-S and EISO-SJ-W summers. The TCCs for all six S2S models are larger for EISO-SJ-S group than for EISO-SJ-W group in all three regions. Specifically, for a three-week lead prediction over the ETP, the averaged improvement of these models in TCC is from 0.11 for EISO-SJ-W group to 0.28 for EISO-SJ-S group, in which the Meteo-France shows the largest increment (from 0.13 to 0.44) while the CMA has the lowest improvement (from 0.08 to 0.15) (green bars in Fig. 2a). Similarly, the averaged TCC increases from 0.05 for EISO-SJ-W group to 0.28 for EISO-SJ-S group over the SWB, in which the ECMWF/NCEP has the largest/lowest improvement (from 0.01 to 0.50 for ECMWF and from 0.17 to 0.20 for NCEP) (green bars in Fig. 2b). Also, the averaged increment is from 0.13 for EISO-SJ-W group to 0.23 for EISO-SJ-S group over NC, in which the NCEP (from 0.12 to 0.27) and CMA (from 0.09 to 0.12) correspond to the maximum and minimum improvements, respectively (green bars in Fig. 2c). Similar differences can be seen clearly in the two-week lead predictions, although the differences between EISO-SJ-S and EISO-SJ-W groups are not as obvious as those in three-week lead predictions (see red bars in Fig. 2a–c).

The RMSEs for all six S2S models are smaller for EISO-SJ-S group than for EISO-SJ-W group. Quantitatively, for a three-week lead prediction over the ETP, the averaged RMSE is reduced from 1.10 for EISO-SJ-W group to 1.05 for EISO-SJ-S group, and the Meteo-France (from 1.03 to 0.92) and ISAC-CNR (from 1.16 to 1.15) have the maximum and minimum reductions, respectively (blue bars in

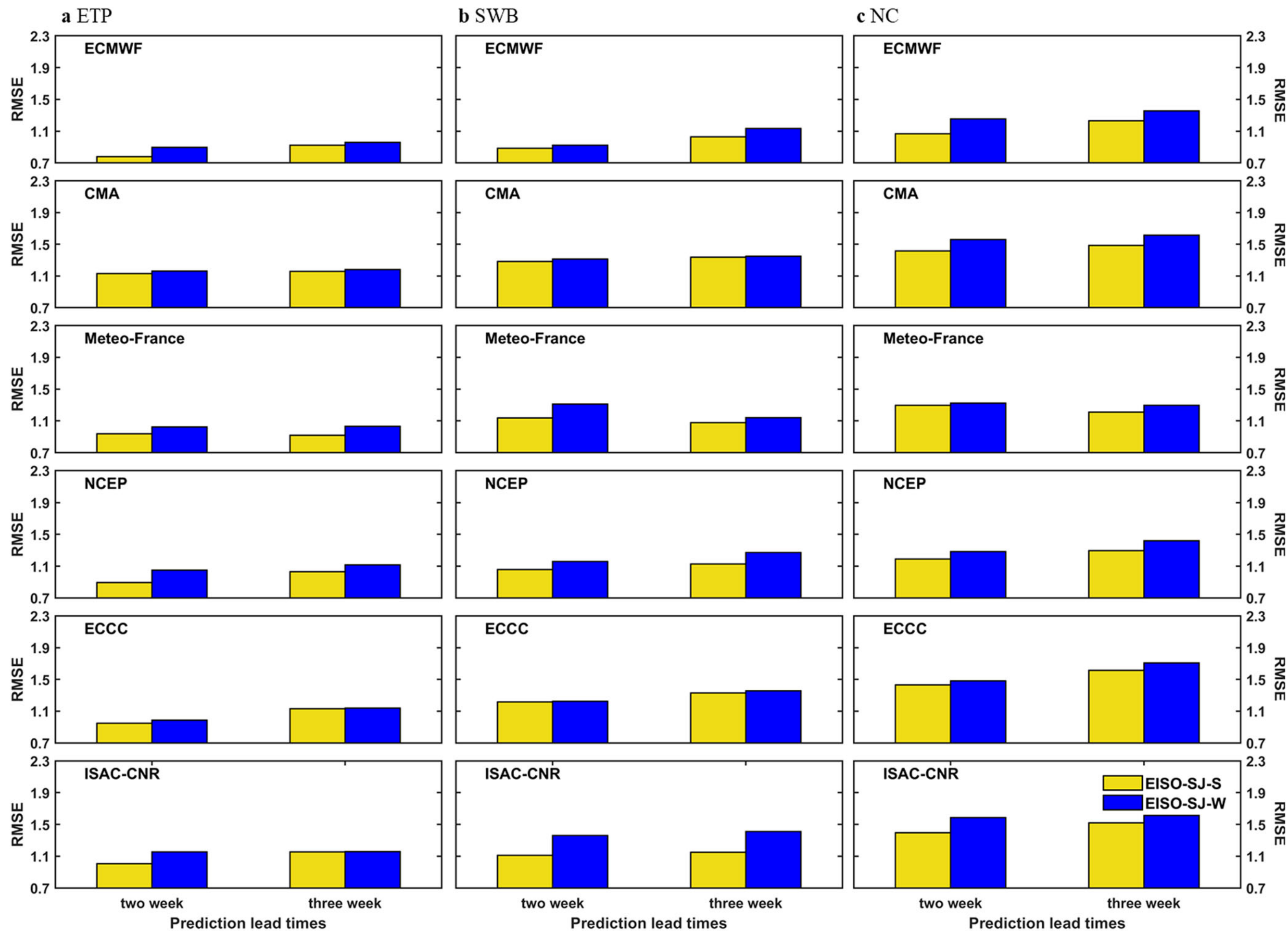

Fig. 3 Subseasonal deterministic prediction over individual typical EA regions: Root Mean Square Error (RMSE). RMSE between the observed weekly SAT anomaly and the predicted ensemble-mean weekly SAT anomaly over the (**a**) ETP, (**b**) SWB, and (**c**) NC with two- and three-week lead times. The yellow (blue) bars show the RMSE for EISO-SJ-S (EISO-SJ-W) group.

Fig. 3a). Over the SWB, the averaged decrease in RMSE from EISO-SJ-W group to EISO-SJ-S group is from 1.28 to 1.17, in which the reduction of ISAC-CNR is the largest (from 1.41 to 1.15) and CMA is the smallest (from 1.35 to 1.34) (blue bars in Fig. 3b). Over NC, the averaged RMSE is decreased from 1.51 for EISO-SJ-W group to 1.39 for EISO-SJ-S group, in which the ECMWF/ISAC-CNR shows the largest/smallest reduction (from 1.36 to 1.23 for ECMWF and from 1.30 to 1.21 for ISAC-CNR) (blue bars in Fig. 3c). Similarly, two-week lead predictions show similar contrasting features (yellow bars in Fig. 3). The unified differences over the three regions for all six S2S models, based on both TCCs and RMSEs, demonstrate that the deterministic prediction skills for the weekly SAT anomaly over EA are significantly better in summers with strong EISO-SJ intensity than in summers with weak EISO-SJ intensity.

The ROC curve is used to comprehensively evaluate model performance in simulating the probability of occurrence of above-normal SAT events. Here, an above-normal SAT event is defined as a weekly SAT warm anomaly of >1 °C (Wu et al. [36]). The ROC curves for the six S2S models for predicted above-normal SAT events over the ETP, SWB, and NC are shown in Fig. 4, respectively, for EISO-SJ-S and EISO-SJ-W groups. Obviously, the six S2S models have larger ROCAs for EISO-SJ-S group than for EISO-SJ-W group over each of the three regions. In terms of the three-week lead prediction over the ETP, the averaged ROCA is 0.57 for EISO-SJ-W group but 0.62 for EISO-SJ-S group, in which the Meteo-France shows the largest increment (from 0.57 to 0.65) while the ECMWF has the lowest improvement (from 0.61 to 0.62) (green solid and dotted lines in Fig. 4a). Over the SWB, the averaged ROCA increases from 0.52 (EISO-SJ-W group) to 0.61 (EISO-SJ-S group), in which the ECCC (from 0.45 to 0.66) and ISAC-CNR (from 0.55 to 0.56) show the largest and lowest improvements, respectively (green solid and dotted lines in Fig. 4b). Over NC, the averaged ROCA increases from 0.53 for EISO-SJ-W group to 0.62 for EISO-SJ-S group, and the ECMWF/CMA shows the largest/smallest increments (from 0.53 to 0.74 for ECMWF and from 0.53 to 0.54 for CMA) (green solid and dotted lines in Fig. 4c). The two-week lead ROCAs show similar differences between EISO-SJ-S and EISO-SJ-W groups (red solid and dotted lines in Fig. 4). We also performed similar analysis for below-normal and normal SAT events, and the results revealed similar differences (Supplementary Fig. 5). The results from the evaluation of probabilistic prediction also clearly exhibited that the prediction skills with two- and three-week lead times are evidently improved when EISO-SJ intensity is enhanced in summer.

Considering that ENSO[37] is the most important mode of interannual variability, which may influence the dependence of subseasonal prediction for EA SAT on the EISO-SJ. Therefore, we reexamined the robustness of the above results after removing ENSO-related summers (Supplementary Table 1 lists the new sample sizes of each model after the elimination of ENSO-related summers). Excluding the impact from ENSO, the subseasonal prediction for SAT even exhibits better skill for EISO-SJ-S group than for EISO-SJ-W group (Supplementary Figs. 6–8). Since the numbers of hindcast year from most S2S models are not large so

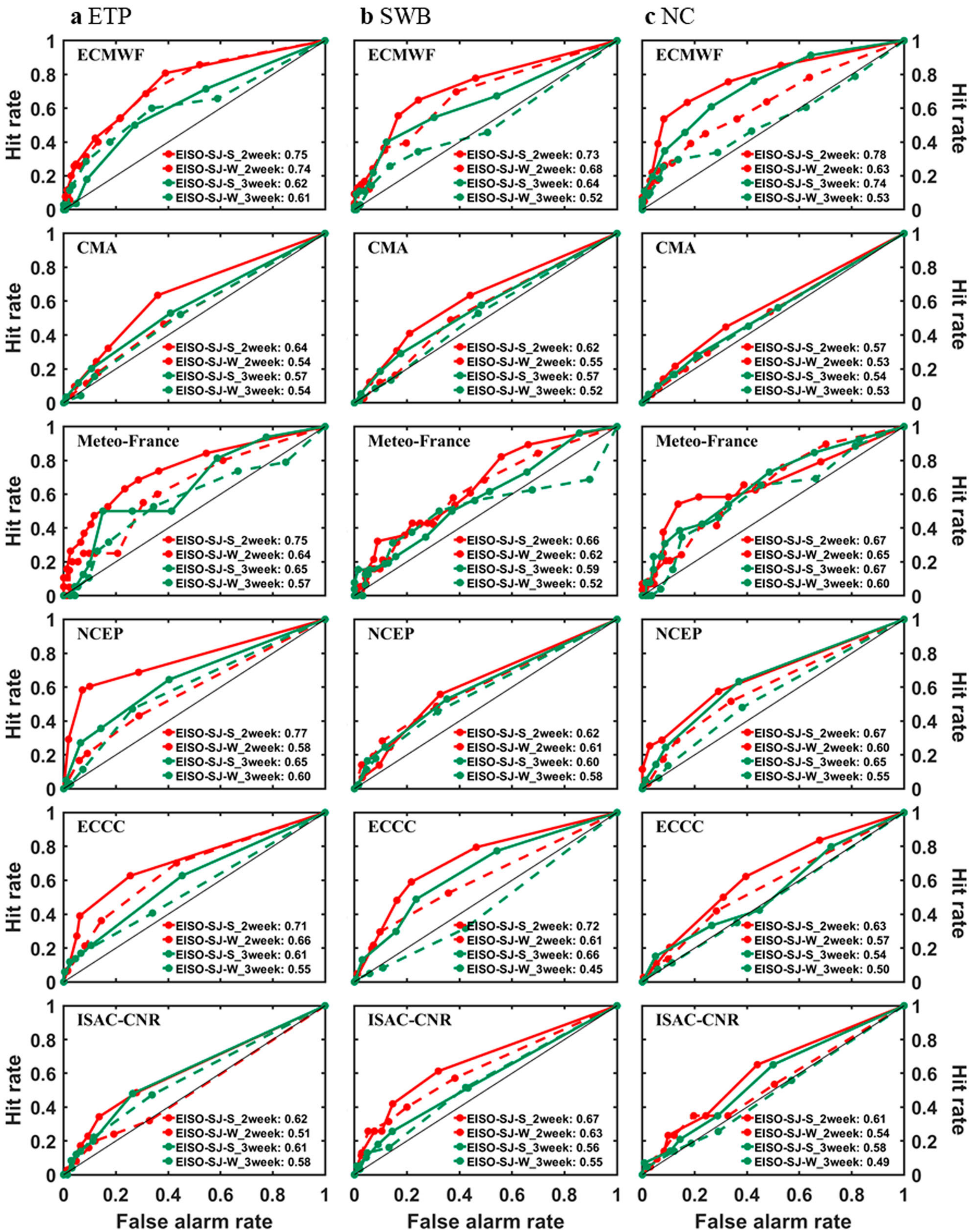

Fig. 4 Subseasonal probabilistic prediction over individual typical EA regions: Relative operating characteristics (ROC). ROC curve for predicting above-normal SAT events over the (**a**) ETP, (**b**) SWB, and (**c**) NC from the six S2S models with two- and three-week lead times for EISO-SJ-S (EISO-SJ-W) group. Here the above-normal SAT events are defined as the weekly SAT anomaly of >1 °C.

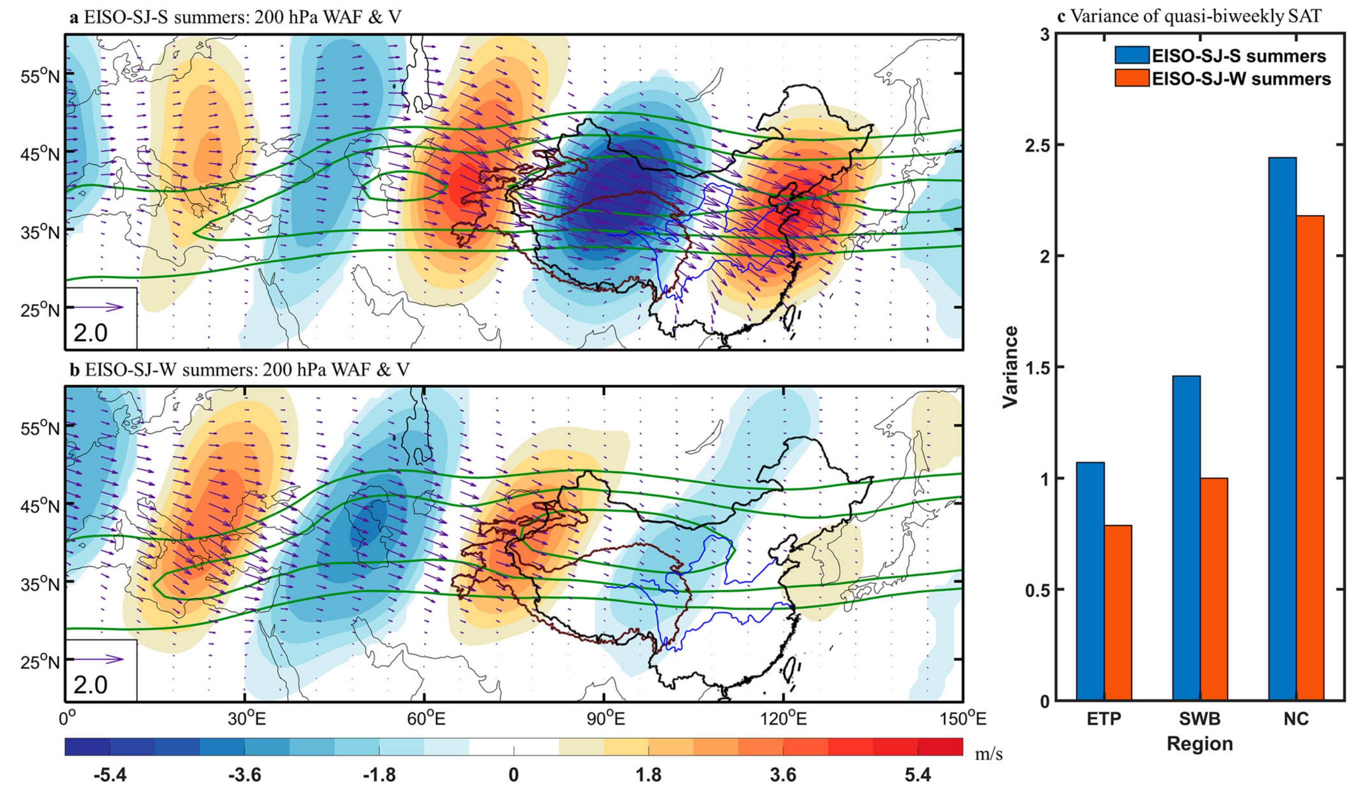

Fig. 5 Quasi-biweekly Rossby wave along the SJ influence on quasi-biweekly EA SAT. Regression maps of boreal summer quasi-biweekly V200 (shading; unit: m s^{-1}) and 200 hPa wave activity flux (WAF; vectors; unit: m^2 s^{-2}) on the first principal component in (**a**) EISO-SJ-S and (**b**) EISO-SJ-W summers. Only values passing the 95% confidence level are plotted. **c** Variance of quasi-biweekly SAT over the ETP, SWB, and NC in EISO-SJ-S (blue bars; unit: °C^2) and EISO-SJ-W summers (orange bars; unit: °C^2).

that the remained sample sizes are small after removing ENSO related interannual variability. Therefore, another way was applied to directly check if the EISO-SJ skill can be obtained from correlations with ENSO. That is, we examined the differences of the subseasonal prediction for SAT over these three regions, respectively, in El Niño- and La Niña-related summers (Supplementary Fig. 9). As a result, their prediction skills do not show any statistically significant differences between the El Niño- and La Niña-related summers in six models. Therefore, from the above two perspectives, the current results indicate that the strong dependence of subseasonal prediction for EA SAT on the EISO-SJ, identified as a new finding in this study, is independent of ENSO.

As a summary, the high agreement among the six S2S models and three target regions, with respect to better prediction skill in summers with strong EISO-SJ intensity in comparison with that in summers with weak EISO-SJ intensity, strongly suggests that the mean state with the amplified quasi-biweekly periodic signals along the SJ evidently increase the regional subseasonal predictability over EA.

DISCUSSION

Previous studies reported that the EISO-SJ mainly features a zonal quasi-biweekly Rossby wave in boreal summer[20,23,34,38]. We therefore considered the empirical orthogonal function for the quasi-biweekly V200 over the SJ region in EISO-SJ-S and EISO-SJ-W summers, and regressed the corresponding quasi-biweekly V200 and 200 hPa wave activity flux on the first principal component, as shown in Fig. 5a and b, respectively. There are clear Rossby waves in both EISO-SJ-S and EISO-SJ-W summers along the SJ, but the more wave activity fluxes propagate eastward along the SJ toward EA, significantly enhancing the quasi-biweekly signals in that regions in EISO-SJ-S summers in comparison with those in EISO-SJ-W summers. Furthermore, the variances of quasi-biweekly SAT are larger over the ETP, SWB, and NC in EISO-SJ-S summers than in EISO-SJ-W summers (Fig. 5c). The results suggest that the quasi-biweekly Rossby wave and the associated energy transport along the SJ are enhanced (reduced) over EA in EISO-SJ-S (EISO-SJ-W) summers, causing stronger (weaker) quasi-biweekly periodic variations in the target regional SAT. This can explain why the two- and three-week lead predictions in the S2S hindcast are improved remarkably in EISO-SJ-S summers.

Table 1. Fractional variance of quasi-biweekly and synoptic SAT and precipitation over the three EA regions.

	SAT		Precipitation	
	Quasi-biweekly	Synoptic	Quasi-biweekly	Synoptic
ETP	36.0%	13.0%	35.2%	33.3%
SWB	45.3%	19.9%	33.3%	41.1%
NC	36.1%	23.2%	27.2%	43.1%

We also performed similar analysis for precipitation, but failed to find significant dependence on EISO-SJ (not shown). We investigated the reason why subseasonal prediction of EA precipitation might be insensitive to EISO-SJ intensity. Table 1 lists the fractional variances of quasi-biweekly and synoptic (i.e., below-8-day) components for SAT and precipitation over the ETP, SWB, and NC. Interestingly, for SAT, the fractional variance of the quasi-biweekly component is much larger than that of the synoptic component (e.g., the three region-averaged quasi-biweekly fractional variance is 39.1%, which is twice that of the synoptic component). For precipitation, however, the fractional variance of the quasi-biweekly component is smaller than that of the synoptic component (31.9% versus 39.2% on average). The above results indicate that the footprint of the atmospheric EISO-SJ on the subseasonal variation of precipitation is not as significant as that on the SAT over EA, which also suggests that subseasonal prediction for EA precipitation is more difficult than that for EA SAT.

METHODS

Observation and reanalysis datasets

Daily atmospheric circulation fields were retrieved from the ERA-Interim dataset provided by the European Centre for Medium-Range Weather Forecasts (ECMWF)[39]. The horizontal resolution of the gridded data was 1.5° × 1.5° and the historical record covered 1982–2018. Daily surface air temperature (SAT) and precipitation data (1982–2018) recorded at 2479 observing stations in China were obtained from the China Meteorological Administration (http://data.cma.cn/en/?r=site/index). Here, boreal summer is defined as May 1 to August 31.

S2S model datasets

For the S2S reforecast data, the hindcast from the database of the S2S prediction project was used[3], in which six models were analyzed: the China Meteorological Administration (CMA), the European Center for Medium-Range Forecast (ECMWF), the Environment and Climate Change Canada (ECCC), the Institute of Atmospheric Sciences and Climate of the National Research Council (ISAC-CNR), the Meteo-France/Centre National de Recherche Meteorologiques (Meteo-France), and the National Centers for Environmental Prediction (NCEP). A detailed description of each of the six models is presented in Supplementary Table 2. Note that the purpose of this study was not to compare model prediction skill, but to understand the dependence of EA subseasonal prediction on the atmospheric EISO-SJ. Therefore, there was no requirement for the reforecast period, frequency of initialization, and ensemble size of the models to be uniform. Also note that the prediction skills for weekly SAT and precipitation were our targets, for which the weekly hindcast data could be obtained from the 7-day mean of the raw prediction data. For example, a two-week (three-week) prediction corresponds to the average of the forecast 11–17 (18–24) days.

Methods

The intraseasonal component of a particular variable can be obtained by the following two steps: (I) removing the slow annual cycle by subtracting the climatological mean and the first three harmonics, and (II) removing the synoptic fluctuations by taking a 5-day running mean. The quasi-biweekly (8–25 days in this study) component can be retrieved easily using the Butterworth bandpass filter. The statistical methods used in this study included empirical orthogonal function analysis and power spectrum analysis. A two-tailed Student's *t* test was used to assess statistical significance. Evaluation methods included the temporal correlation skill (TCC), root mean square error (RMSE), and relative operating characteristics (ROC) curve, which are the primary and most commonly used methods for evaluating the prediction skill of S2S models[36,40,41]. A larger (smaller) TCC (RMSE) value represents better deterministic prediction skill, and a larger value of the area under the ROC curve (named ROCA), denotes better probabilistic prediction skill. Full details of the calculation methods can be found in Supplementary Table 3 and Supplementary Eq. (1) and Supplementary Eq. (2). Two-dimensional wave activity flux, which is used to represent the energy dispersion of a Rossby wave, was calculated with reference to Takaya and Nakamura[42].

DATA AVAILABILITY

The ERA-Interim reanalysis data can be freely accessed via http://apps.ecmwf.int/datasets/data/interim-full-daily/levtype=sfc/. The S2S hindcast data are available from https://apps.ecmwf.int/datasets/data/s2s/levtype=sfc/type=cf/. And the SAT and precipitation data recorded at 2479 observing stations are from http://data.cma.cn/en/?r=site/index (only available by the registered members), and are also obtained from the backup address (IP: 172.16.212.233:~/mnt/2479_station).

CODE AVAILABILITY

All codes for the analysis of this paper are available from the corresponding author upon reasonable request.

Received: 11 December 2022; Accepted: 15 May 2023;
Published online: 27 May 2023

REFERENCES

1. National Academies of Sciences, Engineering and Medicine. *Next Generation Earth System Prediction: Strategies for Subseasonal to Seasonal Forecasts.* (The National Academies Press, Washington, DC, 2016).
2. Robertson, A. W., Kumar, A., Peña, M. & Vitart, F. Improving and promoting subseasonal to seasonal prediction. *Bull. Am. Meteorol. Soc.* **96**, ES49–ES53 (2015).
3. Vitart, F. et al. The subseasonal to seasonal (S2S) prediction project database. *Bull. Am. Meteorol. Soc.* **98**, 163–173 (2017).
4. Merryfield, W. J. et al. Current and emerging developments in subseasonal to decadal prediction. *Bull. Am. Meteorol. Soc.* **101**, E869–E896 (2020).
5. Leung, Y. F. Recreation ecology research in East Asia's protected areas: Redefining impacts? *J. Nat. Conserv.* **20**, 349–356 (2012).
6. Liang, P. & Lin, H. Sub-seasonal prediction over East Asia during boreal summer using the ECCC monthly forecasting system. *Clim. Dyn.* **50**, 1007–1022 (2018).
7. Liu, F. et al. Intraseasonal variability of global land monsoon precipitation and its recent trend. *NPJ Clim. Atmos. Sci.* **5**, 30 (2022).
8. Lin, H. Predicting the dominant patterns of subseasonal variability of wintertime surface air temperature in extratropical northern hemisphere. *Geophys. Res. Lett.* **45**, 4381–4389 (2018).
9. Wu, J., Li, J., Zhu, Z. & Hsu, P.-C. Factors determining the subseasonal prediction skill of summer extreme rainfall over southern China. *Clim. Dyn.* **60**, 443–460 (2023).
10. Martin, G. M. et al. Predictability of South China Sea summer monsoon onset. *Adv. Atmos. Sci.* **36**, 253–260 (2019).
11. Orsolini, Y. J. et al. Impact of snow initialization on sub-seasonal forecasts. *Clim. Dyn.* **41**, 1969–1982 (2013).
12. Li, J., Li, F. & Wang, H. Subseasonal prediction of winter precipitation in southern China using the early November snowpack over the Urals. *Atmos. Ocean. Sci. Lett.* **13**, 534–541 (2020).
13. Zeng, D. & Yuan, X. Multiscale land-atmosphere coupling and its application in assessing subseasonal forecasts over East Asia. *J. Hydrometeorol.* **19**, 745–760 (2018).
14. Xie, J., Yu, J., Chen, H. & Hsu, P.-C. Sources of subseasonal prediction skill for heatwaves over the Yangtze River Basin revealed from three S2S models. *Adv. Atmos. Sci.* **37**, 1435–1450 (2020).
15. Xue, Y. K. et al. Impact of Initialized Land Surface Temperature and Snowpack on Subseasonal to Seasonal Prediction Project, Phase I (LS4P-I): organization and experimental design. *Geosci. Model Dev.* **14**, 4465–4494 (2021).
16. Choi, J. & Son, S. Stratospheric initial condition for skillful surface prediction in the ECMWF model. *Geophys. Res. Lett.* **46**, 12556–12564 (2019).
17. Vimont, D. J., Battisti, D. S. & Hirst, A. C. Footprinting: a seasonal connection between the tropics and mid-latitudes. *Geophys. Res. Lett.* **28**, 3923–3926 (2001).
18. Zhang, T., Huang, B., Yang, S. & Kinter, J. L. Predictable patterns of the atmospheric low-level circulation over the Indo-Pacific Region in Project Minerva: seasonal dependence and intraensemble variability. *J. Clim.* **31**, 8351–8379 (2018).
19. Watanabe, T. & Yamazaki, K. Influence of the anticyclonic anomaly in the subtropical jet over the Western Tibetan Plateau on the intraseasonal variability of the summer Asian monsoon in early summer. *J. Clim.* **25**, 1291–1303 (2012).
20. Yang, J. et al. Characterizing two types of transient intraseasonal oscillations in the Eastern Tibetan Plateau summer rainfall. *Clim. Dyn.* **48**, 1749–1768 (2017).
21. Zhong, S., Wang, H., Chen, B. & Chen, H. Modulation of the atmospheric heat source over the Tibetan Plateau on the intra-seasonal oscillation of summer precipitation in the Yangtze-Huaihe River Basin. *Atmos. Ocean.* **60**, 600–612 (2022).
22. Chan, J. C. L., Wi, W. & Xu, J. Mechanisms responsible for the maintenance of the 1998 South China Sea Summer Monsoon. *J. Meteor. Soc. Jpn.* **80**, 1103–1113 (2002).

23. Fujinami, H. & Yasunari, T. Submonthly variability of convection and circulation over and around the Tibetan Plateau during the boreal summer. *J. Meteor. Soc. Jpn*. **82**, 1545–1564 (2004).
24. Li, J., Zhai, P., Mao, J., Song, L. & Xiao, Q. Synergistic effect of the 25-60-day tropical and midlatitude intraseasonal oscillations on the persistently severe Yangtze floods. *Geophys. Res. Lett*. **48** (2021).
25. Qi, X. & Yang, J. Extended-range prediction of a heat wave event over the Yangtze River Valley: role of intraseasonal signals. *Atmos. Ocean. Sci. Lett.* **12**, 451–457 (2019).
26. Yan, Y., Liu, B. & Zhu, C. Subseasonal predictability of South China Sea summer monsoon onset with the ECMWF S2S forecasting system. *Geophys. Res. Lett*. **48** (2021).
27. Yan, Y. et al. Subseasonal forecast barrier of the North Atlantic oscillation in S2S models during the extreme mei-yu rainfall event in 2020. *Clim. Dyn.* **58**, 2913–2925 (2022).
28. Yang, L. & Zhang, Q. Anomalous perturbation kinetic energy of Rossby Wave along East Asian Westerly Jet and its association with summer rainfall in China. *Chin. J. Atmos. Sci.* **31**, 586–595 (2007).
29. Teng, H. & Wang, B. Interannual variations of the boreal summer intraseasonal oscillation in the Asian-Pacific region. *J. Clim.* **16**, 3572–3584 (2003).
30. Moon, J.-Y., Wang, B. & Ha, K.-J. ENSO regulation of MJO teleconnection. *Clim. Dyn.* **37**, 1133–1149 (2011).
31. Qin, M., Li, S., Xue, Y. & Han, Z. Intraseasonal variability modes of winter surface air temperature over central Asia and their modulation by Greenland Sea ice and central Pacific El Nino-Southern Oscillation. *Int. J. Climatol*. **42**, 8040–8055 (2022).
32. Watanabe, T. & Yamazaki, K. The upper-level circulation anomaly over Central Asia and its relationship to the Asian monsoon and mid-latitude wave train in early summer. *Clim. Dyn.* **42**, 2477–2489 (2014).
33. Gao, M. et al. How are heat waves over Yangtze River valley associated with atmospheric quasi-biweekly oscillation? *Clim. Dyn.* **51**, 4421–4437 (2018).
34. Zhu, T., Yang, J., Wang, B. & Bao, Q. Boreal summer extratropical intraseasonal waves over the Eurasian continent and real-time monitoring metrics. *J. Clim*. **36**, 3971–3991 (2023).
35. Harnos, K. J., L'Heureux, M., Ding, Q. & Zhang, Q. Skill of seasonal Arctic Sea ice extent predictions using the North American multimodel ensemble. *J. Clim.* **32**, 623–638 (2019).
36. Wu, J., Ren, H., Zhang, S., Liu, Y. & Liu, X. Evaluation and predictability analysis of seasonal prediction by BCC second-generation climate system model. *Chin. J. Atmos. Sci.* **41**, 1300–1315 (2017).
37. Bjerknes, J. Atmospheric teleconnection from the equatorial Pacific. *Mon. Weather Rev.* **97**, 163–172 (1969).
38. Yang, J. et al. Distinct quasi-biweekly features of the subtropical East Asian monsoon during early and late summers. *Clim. Dyn.* **42**, 1469–1486 (2014).
39. Dee, D. P. et al. The ERA-Interim reanalysis: configuration and performance of the data assimilation system. *Q.J.R. Meteorol. Soc.* **137**, 553–597 (2011).
40. Black, J. et al. The predictors and forecast skill of northern hemisphere teleconnection patterns for lead times of 3-4 weeks. *Mon. Weather Rev.* **145**, 2855–2877 (2017).
41. Osman, M. & Alvarez, M. S. Subseasonal prediction of the heat wave of December 2013 in Southern South America by the POAMA and BCC-CPS models. *Clim. Dyn.* **50**, 67–81 (2018).
42. Takaya, K. & Nakamura, H. A formulation of a phase-independent wave-activity flux for stationary and migratory quasigeostrophic eddies on a zonally varying basic flow. *J. Atmos. Sci.* **58**, 608–627 (2001).

ACKNOWLEDGEMENTS

J.Y. and T.Z. were supported by funds from the National Natural Science Foundation of China (Grant Nos. 42022034, 42261144671). The authors are grateful for the high-performance computing support from the Center for Geodata and Analysis, Faculty of Geographical Science, Beijing Normal University.

AUTHOR CONTRIBUTIONS

J.Y. conceived the study. T.Z. processed data and drew the figures. T.Z. and J.Y. analyzed the results. F.V. gave the professional guidance and constructive suggestions. All the authors discussed the concepts. The manuscript was drafted by T.Z. and J.Y. and edited by all authors.

COMPETING INTERESTS

The authors declare no competing interests.

ADDITIONAL INFORMATION

Supplementary information The online version contains supplementary material available at https://doi.org/10.1038/s41612-023-00384-5.

Correspondence and requests for materials should be addressed to Jing Yang.